33rd European Study Group with Industry
14 – 18 September 1998
pp. 37 – 55

Thermally Pressing Corner Profiles

Tim Myers
Sjoerd W. Rienstra
TU Eindhoven
Department of Mathematics
P.O. Box 513 5600 MB Eindhoven, The Netherlands

with contributions from:

Jon Chapman, Warrick Cooke, Christian van Enckevort,
Michael Lee, Chris Stolk, Fons van de Ven.

1. Introduction

Trespa International B.V. (Weert, The Netherlands) is a manufacturer of high quality panel material for exterior and interior uses, made of polymerized resin, reinforced with wood fibres or sulphate paper. Typical applications are office desk tops and facade cladding.

The production process starts with impregnating large sheets of paper with resin. Then a pile of sheets of 8–13 mm is pressed together under high pressure (90 bar) in a mould until all of the air is squeezed out. In simplistic terms, the pressing of a plate occurs in two distinct stages; compression followed by heating. This is depicted in Figure 1, where the curves show the product

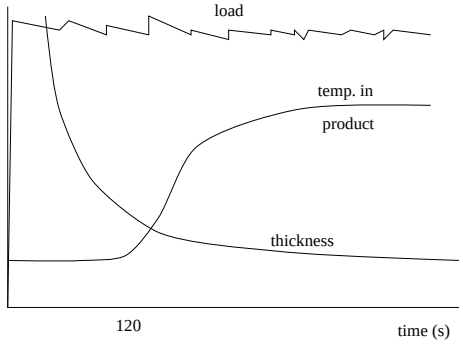

Figure 1. Typical thickness, temperature and loading curves.

thickness, temperature and applied load over time. During the first stage of the process, which last approximately two minutes, the components are compressed to within 10% of the final thickness. During this stage very little heat has reached the components. During the second stage the temperature reaches a critical value and the resin starts to polymerize, eventually resulting in the

solidification of the melt. During polymerization water is formed, which is partly dissolved in the polymer and fibers, partly squeezed out sideways, and partly evaporated through the upper and lower surfaces.

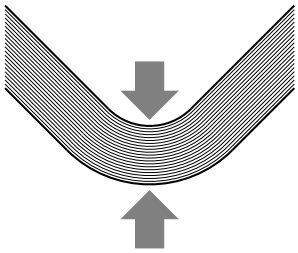

FIGURE 2. The corner profile

The majority of the production involves the manufacture of large rectangular flat plates. Here, the process is well controlled, with little failure losses. A minority of the production consists of, so-called, corner profiles, where a two-dimensional corner (legs of 30 cm, a lateral extension of 4 m) is made by heat-pressing a pile of sheets, folded into a corner shaped mould (figure 2). The upper and lower surfaces of the legs are not exactly parallel. The angle between the legs of the inner mould is 90°, and of the outer mould 91.5°, which is a small but critical amount more. In this way the mould slightly diverges, such that it closes first in the corner, while the contact area between the sheets moves from the corner into the legs. The legs are connected by circular arcs of 10 mm (inner) and 20 mm (outer) radius. This shape may be modified if necessary.

The process of pressing a corner profile is less stable than the regular flat panel process. Density variations and surface blisters have been observed that are supposedly due to captured air and water.

The question is to explain or clarify, by suitable mathematical modelling, the physical processes leading to this adverse behaviour, and to suggest (ways to obtain) more favourable mould shapes.

2. MODELS

We will adopt the hypothesis here that the reduced structural quality is primarily caused by captured air bubbles and not, for example, by chemical changes of material. Therefore, the models used will be centered around the mechanical side of the processes, where bubbles might play a rôle. They are described by the fluid mechanical (resin) and elasto-mechanical behaviour (polymer) of the material.

It is believed that the bubbles are trapped mainly because, when compressed, the material closes in such a way that the induced pressure is not conducive to expelling the trapped air. A description of the actual trapping of bubbles is evidently very difficult, as it requires a kinematical or even dynamical model of a non-continuous material. A better approach, feasible but

requiring a more in-depth research, would be a mixture model [7]. For the moment, however, we will remain, for simplicity, with single component models, probably valid when the trapped air bubbles are small. Therefore, we will evaluate below the following two models: one describing the viscous flow part, and one describing the elastic solid part. At this moment it is not clear yet which description will be most relevant to the original questions. On the one hand, the flow of the heated resin and the trapping of bubbles is a process for which nothing but a viscous model appears to be appropriate. On the other hand, the resin polymerizes, and during the pressing process mainly air (and very little resin) is driven out of the (open!) sides, which suggests that a solid (elastic) model might be in order.

3. Viscous considerations

3.1. Introduction

As previously mentioned, the pressing occurs in two distinct stages, compression followed by curing. The following section is concerned only with the first part of the production process, the compressing stage. In particular the viscous flow of the resin is investigated. The first model described deals with the shearing effect caused by the relative motion of the paper sheets, to determine whether this can tear the paper and lead to cracks appearing. The second model deals with the viscous squeeze flow. The reason for studying this is that it is assumed a considerable part of the densification is due to air bubbles being forced out of the resin. This is backed up by experimental observations of vapor being ejected, although little resin is seen to be ejected. However, it is quite likely that the viscous resin is pushed into the paper and trapped (or at least considerably slowed down). Air bubbles may not take the same path, either because their surface tension makes it more difficult to push air through the narrow paper pores or that air may simply move more rapidly between the paper layers and so be more easily ejected before becoming trapped.

To remove trapped air bubbles the pressure gradient must be reasonably large and acting to push the fluid outwards, to force the bubbles through the viscous resin to the edge of the plates. For this reason the pressure profile in the resin layer is sought. The complication of the resin being forced into the paper is not investigated here, however, an analysis of this situation may be found in [1].

3.2. Cracking due to shear?

During compression of a corner piece there must be some relative motion of the paper layers as the composite adjusts from a flat shape to a curved one. The only significant force opposing this motion is the viscous resistance of the resin. In this section an order of magnitude study is carried out to determine whether this shear force is sufficient to tear the paper and so produce cracks in the finished product.

Geometrical considerations indicate that the relative distance, L, moved by

two adjacent sheets of paper bending to a right angle is

$$L \sim \tfrac{1}{4}\pi(r_2 - r_1), \tag{1}$$

where r_1 and r_2 are the radii of curvature of the paper sheets. In the current

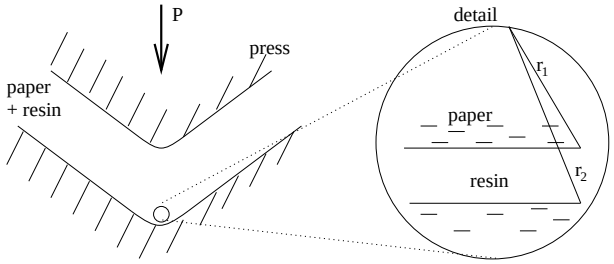

FIGURE 3. Geometry for pressing a corner piece.

problem the radius of curvature of the corner is typically 10 mm, the thickness of the resin layer is 10 μm. Hence locally the problem can be considered as one of Couette flow, see Figure 3. In which case standard viscous flow theory indicates that the shear stress in the fluid is constant and given by

$$\tau = \frac{\eta U}{H}, \tag{2}$$

where η is the viscosity and H is the distance between the two surfaces, $H \sim r_2 - r_1$. The velocity U is given by the length-scale L divided by the time-scale for the flow, which is here taken as 10 s. This leads to

$$\tau = \frac{\eta}{H}\frac{\pi \cdot H}{4 \cdot 10} = \frac{\pi\eta}{40}\ , \tag{3}$$

so the shear stress is independent of the layer thickness. A typical value for the resin viscosity is 2000 cP or 2 Pa s, so the shear stress is of the order 0.16 N/m. Trespa quote the breaking stress of the paper used in the pressing process as 20×10^6 N/m^2, a sheet of thickness 100 μm therefore requires 2×10^3 N/m to tear it. The analysis therefore shows that the stress caused by the shearing of the resin is considerably smaller than that required to tear the paper and it is highly unlikely cracks will appear due to this mechanism.

3.3. Viscous squeezing problem

As the plates compress the resin/paper composite a viscous squeeze film will occur between each pair of paper sheets and the resin will be forced either into the sheets or outwards. To understand the compression of the composite, it is first necessary to understand the basic component of the system, a fluid being squeezed by the normal motion of two solid surfaces. This is the focus of the present section. The main aim of the analysis is to determine the pressure gradient within a resin layer, since this will act to expel (or retain) air bubbles.

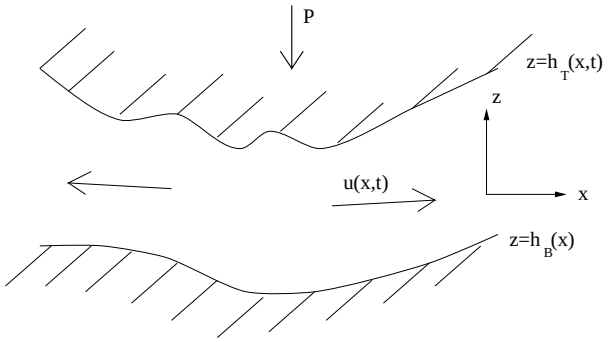

FIGURE 4. A viscous fluid squeezed between two plates located at $z = h_T(x,t)$, $z = h_B(x)$.

Consider the problem of a viscous fluid being squeezed between two solid surfaces, as depicted in Figure 4. Without loss of generality the bottom surface can be assumed stationary, whilst the top one moves under a load P, which may vary with time.

In 2-D the standard lubrication approximation reduces the Navier-Stokes equations to

$$\frac{\partial p}{\partial x} = \eta \frac{\partial^2 u}{\partial z^2}, \tag{4}$$

$$\frac{\partial p}{\partial z} = 0. \tag{5}$$

The continuity equation remains unchanged under this approximation:

$$\frac{\partial \rho}{\partial t} + \frac{\partial (\rho u)}{\partial x} + \frac{\partial (\rho w)}{\partial z} = 0 \ . \tag{6}$$

Appropriate boundary conditions for the velocities u and w are

$$u(h_T) = u(h_B) = 0, \tag{7}$$

$$w(h_B) = 0, \qquad w(h_T) = \frac{\partial h_T}{\partial t} \ , \tag{8}$$

where $h_T(x,t)$ and $h_B(x)$ are the positions of the top and bottom surfaces. Equations (7) and (8) specify no-slip on the solid surfaces. The pressure must be ambient at either end of the contact, *i.e.* $p(\pm L) = p_a$. In the following the ambient pressure will be set to zero. The total load P is the integral of the pressure over a surface $P = \int_{-L}^{L} p(x)\,\mathrm{d}x$. The density is assumed to depend only on pressure and so $\rho(\pm L) = \rho_a$.

Equation (5) indicates $p = p(x,t)$ and hence $\rho = \rho(p) = \rho(x,t)$. Equation (4) may be integrated immediately to give the velocity

$$u = \frac{1}{2\eta} \frac{\partial p}{\partial x} (z - h_B)(z - h_T). \tag{9}$$

Integrating the continuity equation between $z = h_T$ and h_B leads to

$$\frac{\partial \rho}{\partial t}(h_T - h_B) + \frac{\partial}{\partial x}\Big[\rho \int_{h_B}^{h_T} u \, \mathrm{d}z\Big] + \rho \frac{\partial h_T}{\partial t} = 0. \tag{10}$$

Substituting for the velocity and rearranging provides the governing equation for the squeeze flow of a compressible fluid:

$$\frac{\partial}{\partial t}\Big[\rho(h_T - h_B)\Big] = \frac{\partial}{\partial x}\Big[\frac{\rho}{12\eta}\frac{\partial p}{\partial x}(h_T - h_B)^3\Big]. \tag{11}$$

For all cases the dependence of the heights on x should be known (the shape of the press) and for simple configurations equation (11) may be solved analytically. Three such scenarios are worked through in the following sections. However, in general, equation (11) will require solving numerically, this is not carried out in the present work.

Incompressible flow between flat plates

To illustrate the method described above, the simplest configuration, that of an incompressible squeeze film between two flat plates, will be described in this section. In which case the position of the plates is described by

$$h_B = 0, \qquad h_T = h(t), \tag{12}$$

and equation (11) reduces to

$$\frac{\partial h}{\partial t} = \frac{\partial}{\partial x}\Big(\frac{h^3}{12\eta}\frac{\partial p}{\partial x}\Big). \tag{13}$$

Since $h = h(t)$ this may be integrated immediately. After applying the symmetry condition $\partial p/\partial x = 0$ at $x = 0$, this gives an expression for the pressure gradient:

$$\frac{\partial p}{\partial x} = \frac{12\eta f x}{h^3}\ , \tag{14}$$

where $f = \partial h/\partial t$. This shows that the pressure gradient increases linearly away from the centre, $p \propto x$. The consequence for bubble motion through the resin is that near the centre there will only be a small force to cause movement and this is where bubbles are most likely to be trapped. Away from the centre the force increases and so bubbles near the edge of a plate are likely to be removed relatively rapidly.

The pressure in the resin can be determined by integrating (14), subject to $p(\pm L) = 0$:

$$p(x,t) = \frac{6\eta f}{h^3}(x^2 - L^2). \tag{15}$$

This still involves the unknown function $f(t)$ which must be determined by the load condition

$$P = \int_{-L}^{L} p \, \mathrm{d}x = -\frac{8\eta f}{h^3}L^3. \tag{16}$$

So the pressure at any time t is given by

$$p(x,t) = \frac{3P}{4L^3}(L^2 - x^2). \tag{17}$$

Note that the load P applied to the top plate is a known quantity, which may vary with time. The film thickness at time t is determined by integrating f. For the case of constant load this leads to the classical expression for the height variation of an incompressible squeeze film

$$h(t) = \left(\frac{1}{h_0^2} + \frac{Pt}{4L^3\eta}\right)^{-1/2}, \tag{18}$$

see [2, 3] for example. With a time-dependent load, as is depicted on Figure 1, the film height equation requires solving numerically.

Another classic example of a squeeze film is the converging/diverging bearing. The diagrams of presses provided by Trespa indicate that this is also a relevant situation to study, however since the analysis is similar to that described above it is not worked through here. The main result of interest is that the pressure in a converging bearing is similar to that of equation (17) but flattened in the centre and steeper near the edges. Consequently, the central pressure gradient is less favourable to removing air bubbles than the flat plate. A diverging profile has the opposite effect.

Quadratic profile plates

As an approximation to the true shape of the plates when manufacturing a corner the relatively simple case of a quadratic profile will be considered in this section:

$$h_T = h(t) + bx^2 \tag{19}$$

$$h_B = ax^2 \ . \tag{20}$$

If the corner sections are thought of as approximately circular, as depicted in Figure 3, with radii r_1 and r_2 then $b \sim 1/2r_1$, $a \sim 1/2r_2$. The physical case of interest to the present study has $r_1 < r_2$, so $a < b$. Again the fluid will be assumed incompressible. To simplify the analysis the z co-ordinate will be shifted to $\zeta = z - bx^2$, so

$$h_T = h(t) \tag{21}$$

$$h_B = (a-b)x^2 = Bx^2 \ . \tag{22}$$

Equation (11) may be integrated, subject to a symmetry condition at $x = 0$, to give the following expression for the pressure gradient:

$$\frac{\partial p}{\partial x} = \frac{12\eta f x}{(h - Bx^2)^3} \ . \tag{23}$$

Due to the symmetrical nature of the problem, the pressure gradient must always be zero at the centre and bubbles are likely to be retained here. Away

from the centre equation (23) shows that when $B > 0$ the pressure gradient will decrease (since $f < 0$) monotonically away from the centre. The possible singularity, when $x = \sqrt{h/B}$, cannot occur since this implies the surfaces have come into contact, which is only possible in infinite time. When $B < 0$ the pressure gradient decreases away from the centre to a minimum at $x = \pm\sqrt{H/5|B|}$ after which it increases to an asymptote at $\partial p/\partial x = 0$. In this case the pressure gradient over most of the central region (except in the vicinity of $x = 0$) is large and should force air out rapidly. However, as the bubbles approach the edge of the contact region the pressure gradient becomes small and it is possible the bubbles may slow down sufficiently here and not be expelled.

Equation (23) can also be integrated analytically to provide an expression for the fluid pressure:

$$p(x,t) = -\frac{3\eta f}{B}\left[\frac{1}{(h-BL^2)^2} - \frac{1}{(h-Bx^2)^2}\right]. \tag{24}$$

As in the previous example this requires integrating to determine f in terms of the applied load P, which in this case is assumed constant. This leads to, for $B < 0$:

$$f = -\frac{P|B|}{3\eta}\frac{h\sqrt{h|B|}(BL^2+h)^2}{\arctan(L\sqrt{|B|/h})(BL^2+h)^2 - \sqrt{h|B|}L(-|B|L^2+h)}, \tag{25}$$

and for $B > 0$:

$$f = \frac{PB}{3\eta}\frac{h\sqrt{hB}(BL^2-h)^2}{\operatorname{arctanh}(BL/\sqrt{hB})(BL^2-h)^2 - \sqrt{hB}L(BL^2+h)}. \tag{26}$$

The position of the top plate is determined by numerical integration of $\partial h/\partial t = f$, with f given by either (25) or (26).

Quadratic/linear plates

As depicted in Figures 2 and 3, a corner profile is closely approximated by an approximately circular central region joined to an outer, straight section. This may be represented approximately by the form

$$\begin{aligned} h_T &= h(t) + bx^2 && && |x| \le l \\ &= h(t) + 2al(|x|-l) + bl^2 && l \le && |x| \le L \\ h_B &= ax^2 && && |x| \le l \\ &= 2al(|x|-l) + al^2 && l \le && |x| \le L\,. \end{aligned} \tag{27}$$

As in the previous section $b \sim 1/2r_1$, $a \sim 1/2r_2$ where r_1, r_2 are the inner and outer radii of curvature of the central region. Shifting the z-coordinate such that

$$\begin{aligned} \zeta &= z - bx^2 && && |x| \le l \\ &= z - 2al(|x|-l) - bl^2 && l \le && |x| \le L \end{aligned} \tag{28}$$

transforms the plate positions to

$$\begin{array}{lll} h_T &= h(t) & \forall x \\ h_B &= (a-b)x^2 & |x| \le l \\ &= (a-b)l^2 \qquad l \le & |x| \le L\ . \end{array} \tag{29}$$

The problem is then reduced to a combination of those of the previous two sections.

Setting $B = a - b$ the pressure gradient in the two regions is determined as

$$\begin{aligned} \frac{\partial p}{\partial x} &= \frac{12\eta f x}{(h - Bx^2)^3} && |x| \le l \\ &= \frac{12\eta f x}{(h - Bl^2)^3} && l \le |x| \le L\ . \end{aligned} \tag{30}$$

Note, the discontinuity in the gradient of h_T and h_B at $x = l$ will be reflected in a discontinuity in the gradient of $\partial p/\partial x$. The corresponding pressure is

$$\begin{aligned} p &= -\frac{3\eta f}{B}\Big(\frac{1}{(h - Bl^2)^2} - \frac{1}{(h - Bx^2)^2}\Big) - \frac{6\eta f(L^2 - l^2)}{(h - Bl^2)^3} && |x| \le l \\ &= -\frac{6\eta f(L^2 - x^2)}{(h - Bl^2)^3} && l \le \quad |x| \le L. \end{aligned} \tag{31}$$

As $l \to 0$ equations (30, 31) reduce to the results for linear plates, as $l \to L$ the quadratic plate results are retrieved. The total load is, for $B < 0$,

$$\begin{aligned} P &= -\frac{3\eta f}{|B|}\frac{\arctan(|B|l/\sqrt{h|B|})(|B|l^2 + h)^2 - \sqrt{h|B|}l(-|B|l^2 + h)}{h\sqrt{h|B|}(|B|l^2 + h)^2} \\ &\quad -\frac{8\eta f(L^3 - l^3)}{(h + |B|l^2)^3}, \end{aligned} \tag{32}$$

for $B > 0$,

$$\begin{aligned} P &= \frac{3\eta f}{B}\frac{\operatorname{arctanh}(Bl/\sqrt{hB})(Bl^2 - h)^2 - \sqrt{hB}l(Bl^2 + h)}{h\sqrt{hB}(Bl^2 - h)^2} \\ &\quad -\frac{8\eta f(L^3 - l^3)}{(h - Bl^2)^3}. \end{aligned} \tag{33}$$

Since $f = \partial h/\partial t$ these provide the equation for the separation of the two plates $h(t)$, which must again be solved numerically.

3.4. Conclusion and results

In section §3.2 a simplified model for the shearing of a paper/resin system was analysed. Assuming Couette flow, an order of magnitude analysis indicates that cracking will not occur due to the shear of the very viscous resin. Since the induced stress is so much smaller than the required breaking stress it is clear that even if modifications are made to model the flow more accurately the changes will never result in a sufficiently large stress to tear the paper.

In §3.3 a squeeze film model is investigated in order to calculate the pressure within the resin. It is assumed that a sufficiently high pressure gradient will act to drive bubbles of trapped gas from the resin, leading to the appropriate densification. Three examples are worked through in §3.3-3.3. The first of these details the classical squeeze film between two flat plates. The problems described in the latter two sections cover quadratic profile plates and a combination of quadratic and linear ones. The analysis of the quadratic and

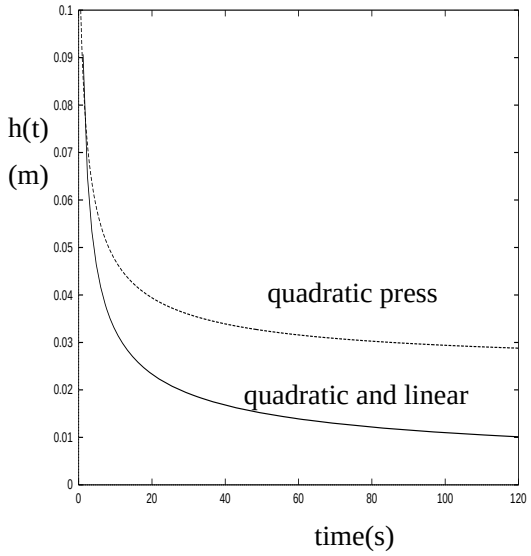

FIGURE 5. Variation of height $h(t)$ for first 120 s.

quadratic/linear profile problems led to an ordinary differential equation for the height $h(t)$, which required solving numerically. The pressure and pressure gradient may then be determined from equations (23, 24, 30, 31).

Figure 5 shows the variation of height $h(t)$ over time for a press with load $P = 100\,\mathrm{N}$, $L = 0.5\,\mathrm{m}$, $l = 0.25\,\mathrm{m}$ and $B = 0.1\,\mathrm{m}^{-1}$ for all three cases discussed earlier. As expected all the height curves decrease in a nonlinear fashion, with an initial rapid decrease followed by a long slow settling period. This is similar to the experimental height decrease displayed in Figure 1. Of the three curves the one corresponding to the linear plate settles most slowly, the quadratic plate settles most rapidly.

The pressure profiles are shown in Figure 6 at time $t = 120\,\mathrm{s}$. The problem of squeezing a fluid between two flat plates leads to a parabolic pressure profile, with a maximum at $x = 0$ of approximately $150\,\mathrm{Pa}$. The quadratic plates, in this example, give a very high pressure near the centre which decreases rapidly to an almost negligible value after $x = 0.35\,\mathrm{m}$. Decreasing the magnitude of B reduces the height of the central peak and increases the value at larger x, until, as $B \to 0$ the linear profile is retrieved. The combination of quadratic and linear plates leads to higher pressures than the purely linear case near the

centre and lower values further out.

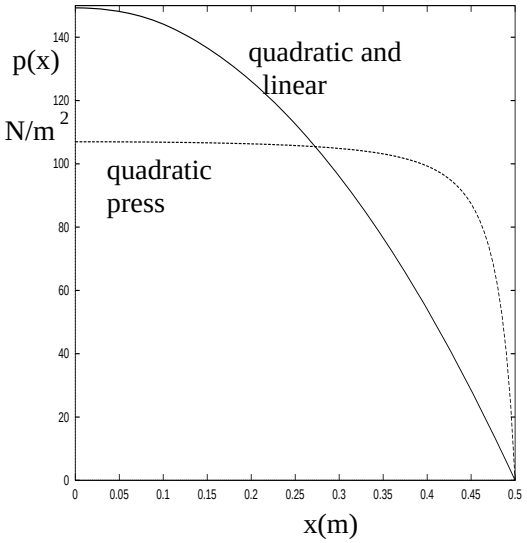

FIGURE 6. Pressure profiles during later stages of pressing process.

The quantity of greatest interest to the present study is the pressure gradient, this is depicted for the three cases in Figure 7. The flat plates show a linearly decreasing pressure gradient which will act to expel air more rapidly the further away it is from the centre. The quadratic plates give a very high pressure gradient over the central region (except in the close vicinity of $x = 0$), which will act to expel air very rapidly from this region. However, further out the pressure gradient becomes very small indicating the possibility of bubbles becoming trapped. Decreasing B will help alleviate this effect. Finally, the linear and quadratic combination incorporates the desirable features of the two separate cases. The pressure gradient is high near the centre. Following the trend of the quadratic plate profile, after reaching a minimum the magnitude decreases until the least effective point for removing air is reached where the linear profile is adopted. After this point the magnitude of the pressure gradient once again increases. With this form of plates there are therefore two likely places for bubble entrapment to occur. The first is at the centre where $\partial p/\partial x = 0$, the second is where the different profiles join and the magnitude of $\partial p/\partial x$ reaches a local minimum value. Adjusting the shape of the curve defined by B and the join position l this minimum value can be altered and so help prevent entrapment in this region. Preliminary calculations indicate that decreasing B (*i.e* making the corner tighter) or increasing l increases the central pressure gradient but reduces the pressure after the join. Increasing B or decreasing l has the opposite effect. The optimal choice will be one which gives an initial rapid rise in the magnitude of the pressure gradient but does not allow the gradient to become too small near the join.

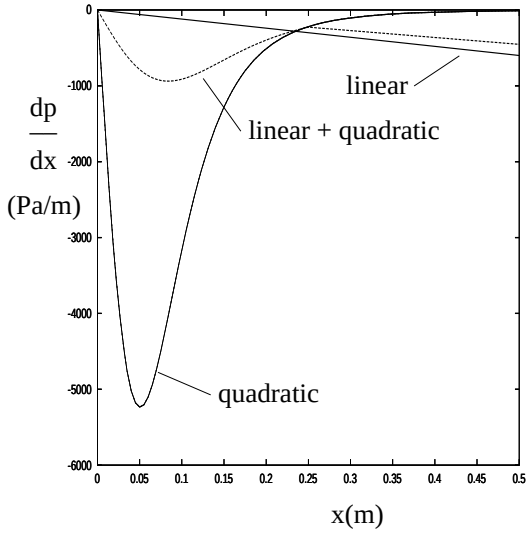

FIGURE 7. Pressure gradients during later stages of pressing process.

The consequences for a press with a converging or diverging form, have not been investigated, although the mathematical model has now been set up to permit this to be carried out relatively easily. However, work on purely converging systems indicates that a converging press will be more likely to entrap air. A diverging one will encourage air removal and this is the type used in practice by Trespa.

Equation (11) sets up the problem for a compressible fluid, however only incompressible examples have been used in the current study. There are two reasons for this, firstly the incompressible problem is considerably simpler, but the main reason is that to close the system a pressure density relation is required. At present there is no information on this. However, the incompressible flow model should indicate the correct trends for pressure and height variation. Further, it is not clear whether the actual fluid is compressed. The current study assumed that the compression effect was due to the removal of air from the resin, the resin will also permeate into the paper. A compressible model would just be imitating this behaviour.

The motion of the bubbles has also not been discussed, except in a very simple manner. Clearly an appropriate pressure gradient will act to move the bubbles, but a relation between the bubble velocity and pressure gradient is still required. To calculate this properly is beyond the scope of this work, however, it is likely that the bubble velocity will be of the same order as the resin velocity. The average resin velocity may be calculated from (9) as

$$\overline{u} = -\frac{\partial p}{\partial x}\frac{(h_T - h_B)^2}{12\eta}. \tag{34}$$

From this it may be estimated how long a bubble will take to travel from a

specified point to the plate edge.

4. Anisotropic elastic solid model

Since the compression or normal stress properties, affected by the captured air bubbles, are expected to be considerably different from the shear stress properties, affected by the layered structure of the paper sheets, the solid phase of the material will be modelled anisotropically, *i.e.* with different Young's moduli in crosswise and lateral directions.

Consider the following geometry (Figure 8). Because of symmetry we only have to consider one half of the profile. The planar part (the leg) occupies the region

$$0 \le x \le L, \quad 0 \le y \le a,$$

while the circular part (the corner area) is given by

$$\begin{aligned} x &= -r\sin(\theta+\theta_1), \quad y = -R + r\cos(\theta+\theta_1), \\ &-\theta_1 \le \theta \le 0, \quad R \le r \le R + a = R_a, \end{aligned}$$

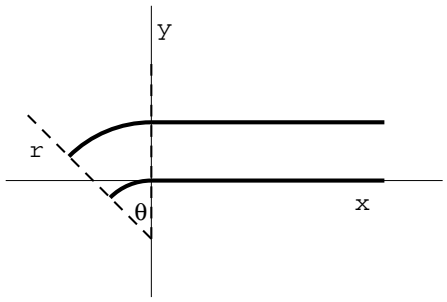

Figure 8. The geometry

where $\theta_1 = \frac{1}{4}\pi$, and R and a are typically 10 mm. The small variations on this geometry (leg angle, etc.), which are supposed to create favourable or unfavourable stress distributions, will for the moment be incorporated by appropriate boundary conditions.

We obtain for the stress tensor $\mathcal{T}$ (with elements t_{ij}) in the planar configuration the following constitutional stress-strain relations [8]

$$t_{xx} = E_L \frac{\partial \xi}{\partial x}, \quad t_{yy} = E_C \frac{\partial \eta}{\partial y}, \quad t_{xy} = G\Big(\frac{\partial \xi}{\partial y} + \frac{\partial \eta}{\partial x}\Big) \tag{35}$$

where $\xi \mathbf{e}_x + \eta \mathbf{e}_y$ is the displacement vector, and the Young's moduli in cross wise (E_C), lateral (E_L) and shear (G) direction are related by

$$2G < E_C \ll E_L.$$

t_{ij} is the stress applied at the side with normal $\mathbf{e}_i$ in direction $\mathbf{e}_j$. The Poisson contraction factor is assumed to be zero: $\nu = 0$. If the material were isotropic, we would have $2G = E_C = E_L$. Boundary conditions will be

$$\begin{aligned} &\text{at} \quad y = 0: && \xi = \eta = 0 \qquad \text{(no slip)},\\ &\text{at} \quad y = a: && \xi = f(x), \quad \eta = -g(x),\\ &\text{for} \quad x \to \infty: && \xi, \eta \to 0. \end{aligned}$$

A suitable first choice will be a simple displacement $f(x) = g(x) = \frac{1}{2}\delta\sqrt{2}$.

In the circular part we have, with $u\mathbf{e}_r + v\mathbf{e}_\theta$ the displacement vector,

$$t_{rr} = E_C \frac{\partial u}{\partial r}, \quad t_{\theta\theta} = E_L\Big(\frac{1}{r}\frac{\partial v}{\partial \theta} + \frac{1}{r}u\Big), \quad t_{r\theta} = G\Big(\frac{\partial v}{\partial r} + \frac{1}{r}\frac{\partial u}{\partial \theta} - \frac{1}{r}v\Big). \tag{36}$$

Boundary conditions will be

$$\begin{aligned} &\text{at} \quad r = R: && u = v = 0 \qquad \text{(no slip)}\\ &\text{at} \quad r = R_a: && u = -\sum W_n \cos(n\theta), \quad v = \sum Z_n \sin(n\theta), \end{aligned}$$

where use is made of the symmetry at $\theta = 0$. A suitable first choice seems to be a simple displacement $u = -\delta\cos\theta$, $v = \delta\sin\theta$.

The two regimes are connected at $x = 0$, $\theta = -\theta_1$ by conditions of continuity: $u = \eta$, and $v = -\xi$.

Because of equilibrium $\mathcal{T}$ must satisfy

$$\nabla \cdot \mathcal{T} = \mathit{I}, \tag{37}$$

in both regions. If we introduce the dimensionless, small, parameters

$$\varepsilon = \frac{E_C}{E_L}, \qquad \gamma = \frac{G}{E_L}, \qquad \text{such that} \quad 2\gamma < \varepsilon \ll 1,$$

and substitute into (37) we find the equations

$$\xi_{xx} + \gamma(\xi_{yy} + \eta_{xy}) = 0, \tag{38a}$$

$$\gamma(\xi_{xy} + \eta_{xx}) + \varepsilon\eta_{yy} = 0, \tag{38b}$$

and

$$\varepsilon u_{rr} + \frac{\varepsilon}{r}u_r - \frac{1}{r^2}u + \frac{\gamma}{r^2}u_{\theta\theta} - \frac{1}{r^2}(1+\gamma)v_\theta + \frac{\gamma}{r}v_{r\theta} = 0 \tag{39a}$$

$$\frac{\gamma}{r}u_{r\theta} + \frac{1}{r^2}(1+\gamma)u_\theta + \frac{1}{r^2}v_{\theta\theta} + \gamma v_{rr} + \frac{\gamma}{r}v_r - \frac{\gamma}{r^2}v = 0 \tag{39b}$$

where subscripts denote a partial derivative.

By expanding ξ and η in a Fourier series in y

$$\xi(x,y) = \sum_{n=1}^{\infty} X_n(x)\sin(ny/a), \qquad \eta(x,y) = \sum_{n=1}^{\infty} Y_n(x)\cos(ny/a), \tag{40}$$

we arrive at

$$\begin{aligned} X_n'' - n^2\gamma X_n - \gamma n Y_n' &= 0 && \text{(41a)} \\ \gamma n(X_n' + Y_n'') - n^2\varepsilon Y_n &= 0 && \text{(41b)} \end{aligned}$$

with solutions, decaying for $x \to \infty$, given by

$$X_n(r) = \sum_{j=1}^{2} A_j \, \mathrm{e}^{\lambda_j x}, \qquad Y_n(r) = \sum_{j=1}^{2} B_j \, \mathrm{e}^{\lambda_j x} \tag{42}$$

where

$$(\lambda_j^2 - n^2\gamma)A_j = \gamma n \lambda_j B_j$$

and $\lambda_{1,2}$ are the two solutions with *negative* real part of

$$\gamma\lambda^4 - (n\epsilon + \gamma^2 n(n-1))\lambda^2 + n^3\gamma^2 = 0.$$

By expanding u and v in a Fourier series in θ

$$u(r,\theta) = \sum_{n=0}^{\infty} U_n(r)\cos(n\theta), \qquad v(r,\theta) = \sum_{n=1}^{\infty} V_n(r)\sin(n\theta), \tag{43}$$

we arrive at

$$\begin{aligned} \varepsilon U_n'' + \frac{\varepsilon}{r}U_n' - \frac{1}{r^2}(1+n^2\gamma)U_n + \frac{n\gamma}{r}V_n' - \frac{n}{r^2}(1+\gamma)V_n &= 0 && \text{(44a)} \\ \gamma V_n'' + \frac{\gamma}{r}V_n' - \frac{1}{r^2}(n^2+\gamma)V_n - \frac{n\gamma}{r}U_n' - \frac{n}{r^2}(1+\gamma)U_n &= 0 && \text{(44b)} \end{aligned}$$

which has the (explicit) solution:

if $n > 1$

$$U_n(r) = \sum_{j=1}^{4} C_j r^{\lambda_j}, \qquad V_n(r) = \sum_{j=1}^{4} D_j r^{\lambda_j} \tag{45a}$$

where

$$\begin{aligned} D_j &= \frac{(1+\gamma+\lambda_j\gamma)(1-\varepsilon\lambda_j^2)}{n(n^2\gamma - 2\gamma - 1)}C_j, \\ & \varepsilon\gamma\lambda^4 - (\varepsilon\gamma + \gamma + \varepsilon n^2)\lambda^2 + \gamma(n^2-1)^2 = 0; \end{aligned}$$

if $n = 0$

$$U_0(r) = C_1 r^{\lambda} + C_2 r^{-\lambda}, \qquad \text{where} \quad \lambda = \sqrt{\frac{1}{\varepsilon}}; \tag{45b}$$

and if $n = 1$

$$\begin{aligned} U_1(r) &= C_1 + C_2\log\Big(\frac{r}{R}\Big) + C_3\Big(\frac{r}{R_a}\Big)^{\lambda} + C_4\Big(\frac{r}{R}\Big)^{-\lambda}, \\ V_1(r) &= D_1 + D_2\log\Big(\frac{r}{R}\Big) + D_3\Big(\frac{r}{R_a}\Big)^{\lambda} + D_4\Big(\frac{r}{R}\Big)^{-\lambda}, \end{aligned} \tag{45c}$$

where $\lambda = \Big(1 + \dfrac{1}{\varepsilon} + \dfrac{1}{\gamma}\Big)^{1/2}$ and

$$(1+\gamma)(D_1+C_1) = -\gamma C_2, \quad D_2 = -C_2,$$

$$\gamma D_3 = \varepsilon(1+\gamma+\lambda\gamma)C_3, \quad \gamma D_4 = \varepsilon(1+\gamma-\lambda\gamma)C_4.$$

An example of a very simple shape, with just $u(R_a) = -\delta\cos\theta$ and $v(R_a) = \delta\sin\theta$ such that we have only the n=1-term, is given in figure 9. The parameters are not chosen from any measurement, but hopefully not too unrealistically: $\varepsilon = 0.03$, $\gamma = 0.01$, $R = 10$, $R_a = 20$, and $\delta = 1$.

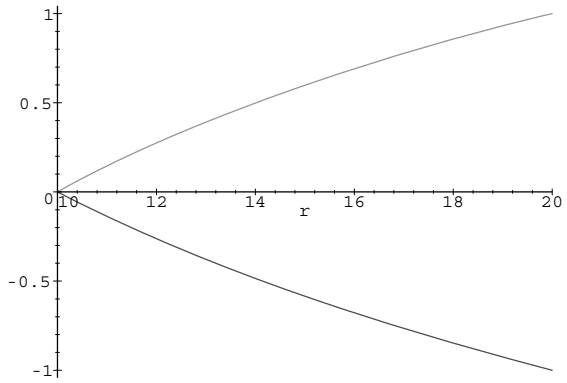

FIGURE 9. $U_1(r)$ and $V_1(r)$ for $10 \le r \le 20$.

A detail of interest is the following boundary layer behaviour. Since ε and γ are small, λ is invariably a large parameter. Consider for example the n=1 -term. Since variable r is always between R and R_a, the term $(r/R)^{-\lambda}$ is practically absent everywhere, except near $r = R$. The same is true for $(r/R_a)^{\lambda}$ near $r = R_a$. This suggests strong gradients in displacement just below the surface of the material, which might well be responsible for residual stresses and hence an uneven surface, maybe even blister formation or cracks in the surface.

This is evidently the result of the relatively low resistance against shear. Any shearing force applied at the surface results into a deformation of the material only near the surface.

Further results are possible only after acquisition of numerical values of the various problem parameters, and the programming and numerical evaluation of the present solution.

5. Relevant literature

The problems described by Trespa have parallels in other industrial processes and, while there was no time to investigate all the areas, it is worth pointing out the relevant literature.

The cracks which appear in the finished product do not occur during the viscous stage and so must occur when the material is hot. In which case it is possible that the cracks appear due to the residual stress calculated in §4 or temperature effects. If temperature variation is the culprit it is well known that thermal stress is proportional to temperature gradient and there are numerous texts on elasticity which describe this [4, 5].

Blistering is a problem frequently encountered in the paint industry and for a similar reason as in the present problem. The paint layer forms a skin which prevents entrapped gas from escaping and so a bubble or blister forms under the skin. A good survey on such problems may be found in [6].

Flow through a porous media, such as paper, has been mentioned already [1]. This work was related to the production of formica. Further information on lubrication flow into a porous media may be found in [2].

References

1. Tayler A.B., Fluid flow between a roller and absorbent compressible paper. *Q. Jl. Mech.Appl. Math* **31**(4) pp. 481-495, 1978.
2. Cameron A., *Basic lubrication theory*, 3rd edition, pp. 143-144. Ellis Horwood 1981.
3. Langlois W.E., *Slow viscous flow*, chapter IX. MacMillan 1964.
4. Love A.E.H., *A treatise on the mathematical theory of elasticity.* Dover 1944.
5. Landau L.D. & Lifshitz E.M., *Theory of elasticity.* Pergammon 1986.
6. Kornum L.O. & Nielsen H.K.R., *Surface defects in drying paint films. Prog. in Org. Coatings* 8 pp. 275–324, 1980.
7. Bowen R.M., Theory of mixtures, *Continuum Physics* **3**, A. Cemal Eringen (eds.), Academic Press. New York 1976.
8. Sokolnikoff I.S., *Mathematical theory of elasticity*, McGraw-Hill, New York 1956.